(Received 25 January 2025, Accepted 24 February 2025, Scheduled 13 March 2025)

Virtual Vector Modulation-Based Model Predictive Control Strategy with Drive Signal Optimization for Quasi-Z-Source Inverter-Fed Permanent Magnet Synchronous Motor System

Yang Zhang[1], Kun Cao[1], Yang Gao[1], Ping Yang[1], Xingwang Chen[1], and Zhun Cheng[2,*]

[1]*Hunan University of Technology, Zhuzhou 412007, China*
[2]*Hunan Railway Professional Technology College, Zhuzhou 412001, China*

ABSTRACT: Aiming at the issues of drive signal errors and high computational complexity in conventional model predictive control, a drive signal optimization virtual vector modulation-based model predictive control (DSO-VVMMPC) strategy with drive signal optimization for quasi-Z-source inverter-fed permanent magnet synchronous motor (QZSI-PMSM) system is proposed in this paper. In the proposed strategy, drive pulses are generated by the combined effect of straight-through voltage vectors (ST VVs) and non-straight-through (NST) VVs over one control period to reduce the ripples of inductor current and stator current. Firstly, the accurate drive signals can be obtained by applying deadbeat algorithm to calculate and correct. The judgment of which sector the reference voltage vector is in and the construction of a cost function for finding the optimal objective are not required. Thus, the computational burden of control system is reduced significantly. In addition, the drive signals are optimized to output to reduce the effect of minimum pulse width on the accuracy of deadbeat algorithm. The steady-state performance of proposed strategy is further improved. Finally, the feasibility and effectiveness of proposed strategy are confirmed by conducting comparative experiments on the RT-LAB experimental platform.

1. INTRODUCTION

Recently, permanent magnet synchronous motors (PMSMs) have been widely used in wind power generation, new energy vehicles, aerospace, and aviation due to their advantages of large speed regulation range, fast response speed, high power density, and high energy conversion efficiency [1–3]. However, voltage-source inverter (VSI) commonly used in conventional PMSM drive systems can only realize voltage reduction function, which is not suitable for occasions with large input voltage variations, so other inverter topologies need to be considered [4]. Quasi-Z-source inverter (QZSI) has the advantages of single-stage boosting and continuous input current, and the existence of straight-through (ST) state eliminates the need to consider the dead time of switching devices, which improves the reliability of the inverter [5, 6]. Therefore, the use of QZSI to drive PMSMs has the advantage of improving energy utilization and reducing system size. However, due to the increase of control variables and the discontinuity of the DC bus voltage, the control process is more complex, and the control effect is unstable [7, 8].

Scholars have proposed many strategies to address this [9]. In [10], a combination of considering complementary sliding mode control as a feedback controller and considering disturbance observer technique as a feed-forward compensator is used to improve the robustness of QZSI-PMSM driven system with external disturbances. In [11], a novel variable dc-chain voltage control method is suggested to regulate the dc-chain voltage indirectly to improve the operation efficiency of the drive system. Model predictive control (MPC) uses a mathematical model to predict the future behavior of the system and design a cost function for optimization with respect to the errors of multiple control variables [12, 13]. It is widely used in areas such as power electronics and motor drives due to its ability to handle nonlinearities and complex constraints [14, 15]. Discrete-time models play a crucial role in MPC. The H_∞ control-based output feedback techniques and unsymmetric Lyapunov function were adopted in [16, 17] to enhance the stability of two-dimensional discrete systems. In conventional MPC, a single voltage vector (VV) is selected by constructing a cost function and using an enumeration method in one control cycle, which results in large steady-state ripple as well as computational burden [18, 19]. To improve the control performance of conventional MPCs, some authors have synthesized and applied virtual VVs through vector modulation. However, this leads to an exponential increase in the number of alternative VVs and an increase in the number of cost function calculations [20].

Currently, reducing the range of candidate vectors by deadbeat algorithm or list method is an effective way to reduce the computational burden of the control system. In [21], each sector is divided into multiple equilateral triangles, and a deadbeat algorithm is applied to reduce the alternative virtual VVs to three. In [22], a hexagonal coordinate system is used to simplify the localization and identification of the created virtual VVs, and the three candidate virtual vectors are selected to be substituted into a cost function to find the optimal. In [23], the

* Corresponding author: Zhun Cheng (120277982@qq.com).

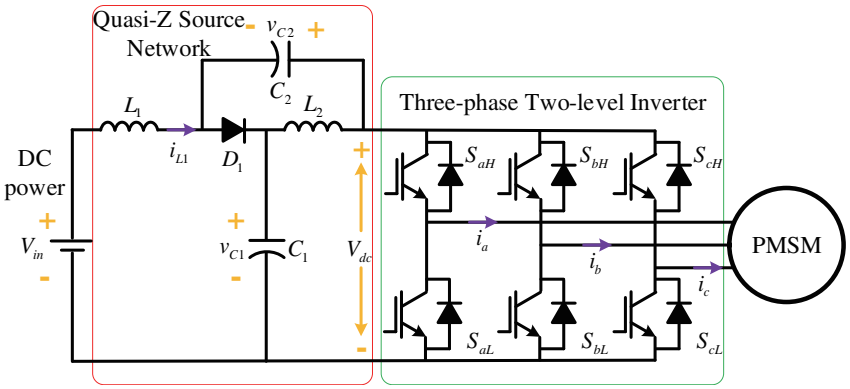

FIGURE 1. The QZSI-PMSM drive system.

virtual VVs are selected by normalizing the reference voltage vector to the first sector, which omits the optimization process. However, it is still necessary to determine the sector where the reference VV is located by the list method and calculate the duty cycle. The concept of hybrid VVs was introduced in [24], which applies the deadbeat principle to compute the action time and then rejects the VVs with action time less than the threshold. The switching frequency is reduced while maintaining steady state performance. However, it needs to calculate the action time again when selecting the dual-vector modulation strategy, which increases the computational burden of the control system. However, the effect of the minimum pulse width on the accuracy of the deadbeat algorithm is not considered. The method proposed in [25] uses virtual vector modulation to directly obtain the duty cycle of the three-phase switching drive pulses. However, the method requires three current predictions, and the effect of the minimum pulse width on the accuracy of the deadbeat algorithm is not considered. In [26], a connection between the control variables on the PMSM-side and QZSI-side is cleverly established by using the duty cycle correction method. Nevertheless, the relationship between duty cycle and minimum pulse width is still overlooked in research.

To address the above problems, a drive signal optimization virtual vector modulation-based model predictive control strategy with drive signal optimization (DSO-VVMMPC) is suggested in this paper. The contribution of this paper is summarized as follows:

1) A virtual vector modulation method is used to generate the driving pulse in one control cycle by employing the combined action of one straight-through (ST) and three non-straight-through (NST) VVs, which effectively reduces the steady-state ripples of inductor current and stator current.

2) Accurate drive signals are directly obtained by decomposing the reference VV and applying a deadbeat algorithm, which effectively reduce the computational burden of the control system.

3) The drive signal optimization method is applied according to the control period and minimum pulse width, which effectively reduces the influence of the minimum pulse width on the accuracy of the deadbeat algorithm.

The remaining sections of this paper are organized as follows. The model of QZSI-PMSM is presented in Section 2. The proposed control strategy is introduced in Section 3. In Section 4, the proposed method is verified by comparative experiments. Finally, the conclusion of this article is given in Section 5.

2. PREDICTIVE MODEL AND CONVENTIONAL MPC

The QZSI-PMSM drive system is shown in Fig. 1, in which the three-phase two-level inverter bridge and quasi-Z-source network form a QZSI, which can provide VVs with different effects. The DC power supply and PMSM act as the energy input and output of the whole system, respectively [26].

2.1. PMSM Model

In this paper, the surface-mounted PMSM is taken as the object of study. The voltage (v_d, v_q) equations of PMSM in a two-phase rotating coordinate system are represented as:

$$\begin{cases} v_d = R_s i_d - \omega_e \psi_q + L_d \dfrac{di_d}{dt} \\ v_q = R_s i_q + \omega_e \psi_d + L_q \dfrac{di_q}{dt} \end{cases} \tag{1}$$

where v_d, v_q, i_d, i_q, L_d, L_q are the stator voltage component, current component, and inductance component of d-q axis; R_s is the stator resistance; ω_e is the electrical angular velocity; and ψ_f is the permanent magnet flux linkage.

Applying first-order Eulerian discretization to (1), the prediction equations of i_d and i_q are represented as:

$$\begin{bmatrix} i_d(k+1) \\ i_q(k+1) \end{bmatrix} = A(k) \begin{bmatrix} i_d(k) \\ i_q(k) \end{bmatrix} + B \begin{bmatrix} v_d(k) \\ v_q(k) \end{bmatrix} + C(k) \tag{2}$$

where

$$\begin{cases} A(k) = \begin{bmatrix} 1 - R_s T_s / L_d & T_s L_q \omega_e(k) / L_d \\ -T_s L_d \omega_e(k) / L_q & 1 - R_s T_s / L_q \end{bmatrix} \\ B = \begin{bmatrix} T_s / L_d & 0 \\ 0 & T_s / L_q \end{bmatrix} \\ C(k) = \begin{bmatrix} 0 \\ -T_s \omega_e(k) \psi_f / L_q \end{bmatrix} \end{cases} \tag{3}$$

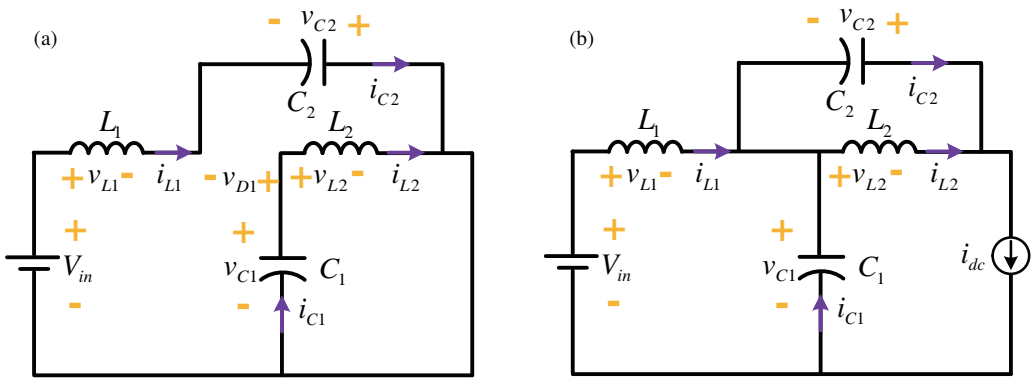

FIGURE 2. Working states of QZSI. (a) ST state, (b) NST state.

where T_S is the sampling period.

2.2. QZSI Model

The operating states of QZSI can be classified into NST and ST states. The equivalent circuits of QZSI at both states are displayed in Fig. 2, where the two inductance values and two capacitance values are equal, respectively ($L_1 = L_2$, $C_1 = C_2$).

It is necessary to predict the future behavior of QZSI in both operating states. The working condition in ST state is shown in Fig. 2(a). At this time, diode D_1 is disconnected; DC power supply V_{in} and capacitor C_2 charge inductor L_1; and capacitor C_1 discharges through inductor L_2. The working condition in NST state is shown in Fig. 2(b). At this time, diode D_1 is closed; DC power supply V_{in} and inductor L_1 charge capacitor C_1; and inductor L_2 charges capacitor C_2. There is $i_{L1} = i_{L2}$ under the condition that $L_1 = L_2$ of $C_1 = C_2$. When the inductor stray resistance is neglected, the state equation of L_1 is expressed as:

$$\begin{cases} L_1 \dfrac{di_{L1}}{dt} = v_{C1}, & ST\ state \\ L_1 \dfrac{di_{L1}}{dt} = V_{in} - v_{C1}, & NST\ state \end{cases} \tag{4}$$

Applying first-order Eulerian discretization to (4), the prediction equations of i_{L1} is expressed as:

$$i_{L1}(k+1) = \begin{cases} i_{L1}(k) + \dfrac{T_S}{L_1} v_{C1}(k), & ST\ state \\ i_{L1}(k) + \dfrac{T_S}{L_1}[V_{in} - v_{C1}(k)], & NST\ state \end{cases} \tag{5}$$

The state equation of C_1 is expressed as:

$$\begin{cases} C_1 \dfrac{dv_{C1}}{dt} = -i_{L1}, & ST\ state \\ C_1 \dfrac{dv_{C1}}{dt} = i_{L1} - i_{dc}, & NST\ state \end{cases} \tag{6}$$

Applying first-order Eulerian discretization to (6), the prediction equation of v_{C1} is expressed as:

$$v_{C1}(k+1) = \begin{cases} v_{C1}(k) + \dfrac{T_S}{C_1}[-i_{L1}(k+1)], & \\ ST\ state & \\ v_{C1}(k) + \dfrac{T_S}{C_1}[i_{L1}(k+1) - i_{dc}(k+1)], & \\ NST\ state & \end{cases} \tag{7}$$

where $i_{dc}(k+1)$ is the DC bus current for next sampling period, and it is obtained from the switching state and output currents of the three-phase inverter bridge:

$$i_{dc}(k+1) = S_{aH} i_a + S_{bH} i_b + S_{cH} i_c \tag{8}$$

where S_{aH}, S_{bH}, and S_{cH} refer to the switching states of the upper bridge arm of the three-phase inverter, respectively.

2.3. Delay Compensation

To improve the performance of the MPC strategy, a two-step prediction method is employed to compensate the delay as follows:

$$\begin{bmatrix} i_d(k+2) \\ i_q(k+2) \end{bmatrix} = A(k) \begin{bmatrix} i_d(k+1) \\ i_q(k+1) \end{bmatrix} + B \begin{bmatrix} v_d(k+1) \\ v_q(k+1) \end{bmatrix} + C(k) \tag{9}$$

$$i_{L1}(k+2) = \begin{cases} i_{L1}(k+1) + \dfrac{T_S}{L_1} v_{C1}(k+1), & \\ ST\ state & \\ i_{L1}(k+1) + \dfrac{T_S}{L_1}[V_{in} - v_{C1}(k+1)], & \\ NST\ state & \end{cases} \tag{10}$$

The method uses the voltage vector $v_{dq}(k)$ applied at moment k to estimate the inductor current of QZSI-side and the stator current of PMSM-side at moment $k+1$.

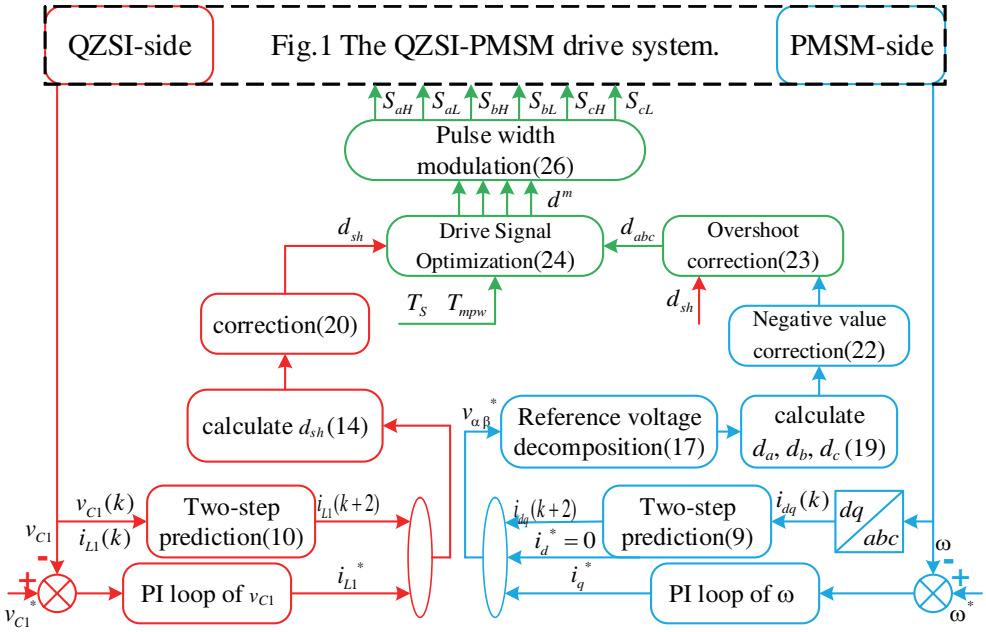

FIGURE 3. Proposed DSO-VVMMPC strategy.

2.4. Cost Function

In conventional MPC strategy, the optimal VV is chosen as the switching state for the next sampling period according to the cost function g, which includes multiple control objectives such as i_{dq} and i_{L1}. It can be defined as:

$$g=|i_d(k+2)-i_d^*|+\left|i_q(k+2)-i_q^*\right|+Q\,|i_{L1}(k+2)-i_{L1}^*| \quad (11)$$

where i_{dq}* and i_{L1}* are the reference values of i_{dq} and i_{L1}, respectively, and Q is the weighting coefficient for the cost function. A cycle of recursion is performed on the nine finite vectors of the two-stage QZSI to minimize the cost function in (11). The optimal vector is then applied in the next control period.

3. PROPOSED DSO-VVMMPC STRATEGY

To optimize the control performance and computational burden of QZSI-PMSM system, while considering the influence of the minimum pulse width on the accuracy of the deadbeat algorithm, a virtual vector modulation-based model predictive control strategy with drive signal optimization (DSO-VVMMPC) is suggested in this paper. This strategy mainly consists of the following parts: calculation of d_{sh}, virtual vector modulation method, and drive signal optimization method, as shown in Fig. 3.

3.1. Calculation of d_{sh}

The ST states include single-phase ST, two-phase ST, and three-phase ST. In this paper, only single-phase ST VVs are used to reduce the switching frequency of proposed DSO-VVMMPC strategy.

If ST and NST VVs are used alternately to generate driving pulses within a control cycle, then (10) needs to be updated as follows:

$$\begin{aligned} i_{L1}(k+2) &= i_{L1}(k+1)+d_{sh}\,[i_{L1}^{st}(k+2)-i_{L1}(k+1)] \\ &\quad +(1-d_{sh})[i_{L1}^{nst}(k+2)-i_{L1}(k+1)] \end{aligned} \quad (12)$$

where d_{sh} is the ST duty cycle of QZSI, as the ratio of the action time of the ST VV in one control cycle to the control period. $i_{L1}^{st}(k+2)$ refers to the predicted value of i_{L1} under the applied ST state from (10), and $i_{L1}^{nst}(k+1)$ refers to the predicted value of i_{L1} under the applied NST state from (10). To ensure that the modulation coefficients of the QZSI-PMSM system do not conflict, the following conditions must be satisfied:

$$\begin{cases} 0 <= d_{sh} < 0.5 \\ 0 <= M + d_{sh} <= 1 \end{cases} \quad (13)$$

where M is the modulation ratio of the system output voltage, as the ratio of the amplitude of the output voltage to 2/3 times the DC bus voltage (V_{dc}).

The calculated value of d_{sh} can be obtained by directly causing the predicted value of i_{L1} at $k+2$ moment in (12) equal to its reference value:

$$d_{sh}=\frac{[i_{L1}^*-i_{L1}(k)]L_1/T_S+v_{C1}(k)-V_{in}}{2v_{C1}(k)-V_{in}} \quad (14)$$

When the system is running stably, the fluctuation of the calculated value of d_{sh} is small, but when the operating conditions suddenly change, the calculated value of d_{sh} may suddenly change and no longer comply with (13). At this point, the following correction needs to be made: when the d_{sh} value is less than 0, make it equal to 0; when the d_{sh} value is greater than 0.5, make it equal to 0.5.

3.2. Virtual Vector Modulation Method

Eight NST VVs and twelve single-phase ST VVs can be provided by the three-phase two-level QZSI. The sector division of the VVs is shown in Fig. 4, where v^* is the reference VV.

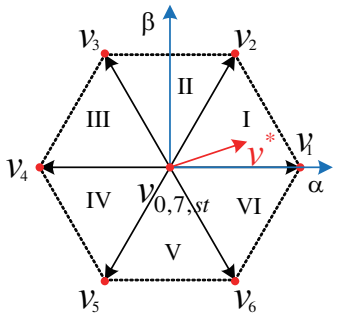

FIGURE 4. Sector division of the VVs.

The reference value of v_{dq} is obtained by causing the predicted value of i_{dq} at $k+2$ moment in (9) equal to its reference value:

$$\begin{bmatrix} v_d^* \\ v_q^* \end{bmatrix} = B^{-1}\left(\begin{bmatrix} i_d^* \\ i_q^* \end{bmatrix} - A(k) \begin{bmatrix} i_d(k+1) \\ i_q(k+1) \end{bmatrix} - C(k) \right) \tag{15}$$

Convert the reference value of v_{dq} to the two-phase stationary coordinate system:

$$\begin{cases} v_\alpha^* = v_d^* \cos\theta - v_q^* \sin\theta \\ v_\beta^* = v_d^* \sin\theta + v_q^* \cos\theta \end{cases} \tag{16}$$

where θ is the rotor position angle.

In the proposed strategy, space vector pulse width modulation (SVPWM) is not used; the process of computing the cost function several times for optimization is omitted; and judging the sector where the reference VV is located is avoided. The accurate drive signal is directly obtained with only one prediction by the virtual vector modulation method, which greatly reduces the computational burden of the control system without losing the computational accuracy.

Firstly, the reference VV is decomposed, and its relationship with the duty cycle of the three-phase VV is presented in the form of a matrix:

$$\begin{bmatrix} v_{1\alpha} & v_{3\alpha} & v_{5\alpha} \\ v_{1\beta} & v_{3\beta} & v_{5\beta} \end{bmatrix} \begin{bmatrix} d_a \\ d_b \\ d_c \end{bmatrix} = \begin{bmatrix} v_\alpha^* \\ v_\beta^* \end{bmatrix} \tag{17}$$

where $v_{1\alpha\beta}$, $v_{3\alpha\beta}$, and $v_{5\alpha\beta}$ are the components of VV v_1, v_3, v_5 in α-β axis, respectively; d_a, d_b, and d_c are the duty cycles of *abc* three-phase respectively, which are the ratios of the inverter three-phase higher bridge arm turn-on and lower bridge arm turn-off time to the whole control cycle. The virtual voltage vector formed by the independent states of each phase satisfies the superposition principle and vector synthesis relationship.

A system of nonhomogeneous linear equations $\boldsymbol{Ax} = \boldsymbol{b}$ is shown in (17). Applying elementary row transformations to its augmented matrix and organizing them yields:

$$(\mathbf{A}|\mathbf{b}) \to \begin{bmatrix} 1 & 0 & -1 & \frac{3v_\alpha^* + \sqrt{3}v_\beta^*}{2V_{dc}} \\ 0 & 1 & -1 & \frac{\sqrt{3}v_\beta^*}{V_{dc}} \end{bmatrix} \tag{18}$$

This system of linear equations has a coefficient matrix $\boldsymbol{A}$ of rank 2, an augmented matrix $(\boldsymbol{A}|\boldsymbol{b})$ of rank 2, and the number of unknowns is 3. Therefore, the system of linear equations has a solution, and the solution is not unique. Its general solution is:

$$[d_a, d_b, d_c]^T = k[1,1,1]^T + \left[\frac{3v_\alpha^* + \sqrt{3}v_\beta^*}{2V_{dc}}, \frac{\sqrt{3}v_\beta^*}{V_{dc}}, 0 \right]^T \tag{19}$$

where k is an arbitrary constant, and k is firstly taken to be 0 to facilitate the calculation. At this time, the initial value of d_c is 0, and the initial values of d_a and d_b are determined by the collection and reference value of the system in current moment.

For different values of k, the zero VVs involved in virtual vector modulation will be different, and the possible cases are: v alone is involved in modulation; v_7 alone is involved in modulation; and both v and v_7 are involved in modulation. But the value of k does not affect the final formation of the reference VV, as shown in Fig. 5.

For QZSI drive systems, it is commonly necessary to insert ST VVs into NST VVs. To facilitate modulation of the voltage vector, d_{sh} can be stripped out beforehand, and the three-phase duty cycle at this time should satisfy the following condition:

$$0 <= d_a,\ d_b,\ d_c <= 1 - d_{sh} \tag{20}$$

The correction calculation process for the three-phase duty cycle is illustrated in Fig. 6. As shown in Fig. 6(a), the initial calculated values of d_a, d_b, and d_c may not satisfy the constraints of (20), so it is necessary to correct them for negative values as shown in Fig. 6(b) and overshooting as shown in Fig. 6(c). Mark the maximum value of the three as d_Z, the minimum value as d_X, and the other one as d_Y

$$\begin{aligned} d_X &= \min\{d_a, d_b, d_c\},\ d_Y = \text{mid}\{\mathrm{d_a}, \mathrm{d_b}, \mathrm{d_c}\}, \\ d_Z &= \max\{d_a, d_b, d_c\} \end{aligned} \tag{21}$$

Firstly, check whether there is a negative value in the three-phase duty cycle, that is, whether d_X is less than 0. Since the initial value of d_c is 0, it has been determined that d_X is a non-positive value. Regardless of its value, the minimum value of the three-phase duty cycle can be directly corrected to 0 by the following operation:

$$d_{x1} = d_x - d_X, \quad x = a, b, c \tag{22}$$

The d_{a1}, d_{b1}, and d_{c1} obtained by negative value correction in Fig. 6(b) are still one of the general solutions of (19), so the above correction action will not affect the amplitude and direction of the reference voltage.

Then, check whether there is overshoot in the three-phase duty cycle, that is, whether $d_Z - d_X$ is greater than $1 - d_{sh}$. If it is judged as no, no correction is required; if the judgment is

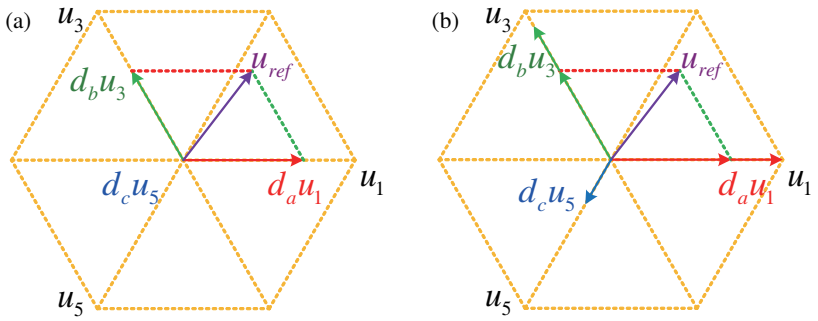

FIGURE 5. Reference VV obtained using different zero vectors. (a) Using v_0. (b) Using v_7.

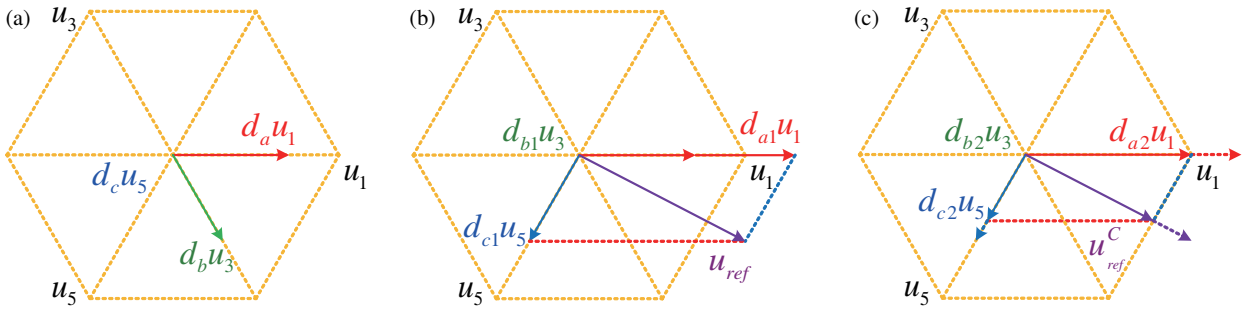

FIGURE 6. Correction of three-phase duty cycle. (a) Initial calculated value. (b) Negative value correction. (c) Overshoot correction.

TABLE 1. Virtual vector modulation strategies.

Different three-phase duty cycle sizes	The sector	Effective VVs involved in modulation	ST VV involved in modulation
$d_c < d_b < d_a$	I	v_1, v_2	v_{st12}
$d_c < d_a < d_b$	II	v_2, v_3	v_{st23}
$d_a < d_c < d_b$	III	v_3, v_4	v_{st34}
$d_a < d_b < d_c$	IV	v_4, v_5	v_{st45}
$d_b < d_a < d_c$	V	v_5, v_6	v_{st56}
$d_b < d_c < d_a$	VI	v_6, v_1	v_{st61}

yes, overshoot correction is required as follows:

$$d_{x2} = \begin{cases} d_{x1} & d_Z - d_X \le 1 - d_{sh} \\ \dfrac{d_{x1}(1-d_{sh})}{d_Z - d_X} & d_Z - d_X > 1 - d_{sh} \end{cases} \quad x = a, b, c \quad (23)$$

The d_{a2}, d_{b2}, and d_{c2} obtained from overshoot correction in Fig. 6(c) are the best alternatives to the general solution of (19) under the constraint condition of (20). The above correction action will not affect the direction of the reference voltage but will affect the amplitude of the reference voltage. Reset the d_{a2}, d_{b2}, and d_{c2} obtained from overshoot correction to d_a, d_b, and d_c.

The virtual vector modulation strategies corresponding to different three-phase duty cycle sizes are summarized in Table 1, including the sector where the reference VV is located, the effective and ST VVs are involved in modulation. The three-phase duty cycle (d_a, d_b, and d_c) and the ST duty cycle (d_{sh}) form the driving signal, which can be modulated to generate driving pulses. The v_{st12} in Table 1 refers to the ST VV that can be inserted between v_1 and v_2, etc.

3.3. Drive Signal Optimization Method

In practical applications, the minimum pulse width (T_{mpw}) is usually set to reduce switching losses. The four driving signals d_{sh}, d_a, d_b, and d_c were calculated in Subsections 3.1 and 3.2, respectively. However, the calculated values of these driving signals are usually not integer multiples of T_{mpw}, and the control circuit will extend the noninteger part of such driving signals to output a complete T_{mpw} or lose it without generating driving pulses. Therefore, it is necessary to optimize the driving signal to reduce the errors caused by such output methods in deadbeat algorithm.

The calculated and output values of the driving signal are shown in Fig. 7, and they are compared with the optimized output values. In Fig. 7(a), d is the calculated value of four driving

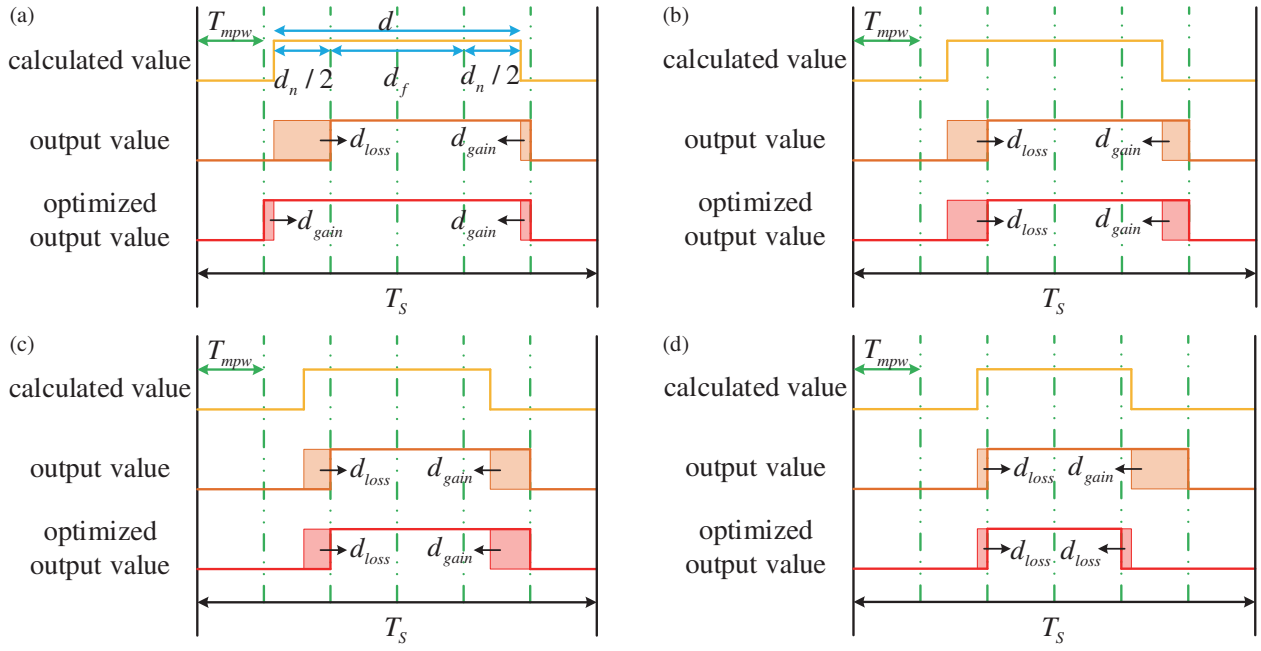

FIGURE 7. Calculated and output values of the driving signal. (a) $3T_{mpw}/2 \le d_n < 2T_{mpw}$, (b) $T_{mpw} \le d_n < 3T_{mpw}/2$, (c) $T_{mpw}/2 \le d_n < T_{mpw}$, (d) $0 < d_n < T_{mpw}/2$.

signals, which can be decomposed into the following two parts: the part that experiences a complete T_{mpw} is defined as d_f, and the part that experiences an incomplete T_{mpw} is define as d_n.

In order to improve the accuracy of the deadbeat algorithm, the driving signal needs to be optimized based on T_{mpw} and control period (T_S) to minimize the error between the optimized output value and the calculated value. The optimization function is defined as follows:

$$\begin{cases} d^m = [\text{round}(\text{dN})]/\text{N} \\ N = T_S/T_{mpw} \end{cases} \tag{24}$$

where d_m is the optimized driving signal; the round function is a rounding function to the nearest integer; and N is the ratio of a control period to the minimum pulse width.

The total error of the drive signal is defined as follows:

$$e_d = |d_{loss} - d_{gain}| \tag{25}$$

where d_{loss} represents the part that the driving signal is lost in one control cycle, and d_{gain} represents the part that the driving signal is extended in one control cycle, consistent with Fig. 7.

According to the size relationship between d_n and T_{mpw}, optimization processing can be divided into four cases, corresponding to (a), (b), (c), and (d) in Fig. 7, respectively. From Figs. 7(a) and (d), it can be seen that in both cases, the total error of the optimized driving signal is significantly reduced compared to that before optimization. From Figs. 7(b) and (c), it can be seen that in both cases, the total error of the optimized driving signal remains consistent with that before optimization. Therefore, the proposed strategy can reduce the total error of the driving signal in deadbeat algorithm.

Because ST VV has the same effect on the stator current of the motor as zero VV, the ST VV is inserted between two effective VVs, and a symmetrical modulation strategy is adopted to reduce the steady-state ripple of the stator current. The driving signals of the six switching tubes of the inverter are as follows:

$$\begin{cases} S_{XH} = (1 - d_X^m)T_S/2 \\ S_{XL} = (1 - d_X^m)T_S/2 \\ S_{YH} = [1 - (d_Y^m + d_{sh}^m)]T_S/2 \\ S_{YL} = (1 - d_Y^m)T_S/2 \\ S_{ZH} = [1 - (d_Z^m + d_{sh}^m)]T_S/2 \\ S_{ZL} = [1 - (d_Z^m + d_{sh}^m)]T_S/2 \end{cases} \tag{26}$$

where the subscript H represents the upper arm of the inverter bridge, and the subscript L represents the lower arm of the inverter bridge.

Taking $d_b < d_c < d_a$ as an example, the reference VV of this control cycle is in sector VI, where the driving pulses are generated by zero VV v, effective VVs v_6 and v_1, and single-phase ST VV v_{st61}, as shown in Fig. 8.

4. EXPERIMENTAL VERIFICATION

The experimental model is constructed and verified on the RT-LAB experimental platform, and the digital signal processor (DSP) adopts TMS320F2812. The RT-LAB experimental platform and RT-LAB in-the-loop system configuration are presented in Fig. 9. The parameters of system are presented in Table 2. K_p and K_i of PMSM speed control loop are respectively set to 12 and 200, while K_p and K_i of the capacitive voltage control loop of the QZSI are respectively set to 0.5 and 50. These values for control strategies are kept constant in all the next experiments.

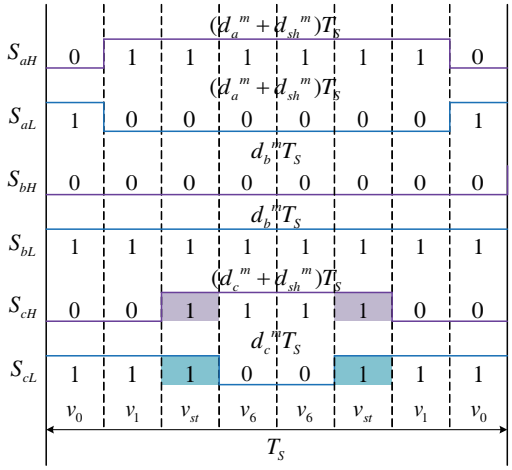

FIGURE 8. Schematic diagram of drive pulses.

Parameter	Value	Unit
Number of pole pairs	4	/
Stator resistance	0.15	Ω
Stator inductance	1.625	mH
Permanent magnet flux	0.1	Wb
Moment of inertia	4.78	g·cm^2
Rated speed	2000	r/min
Rated torque	15	N·m
Z-Source Capacitor	470	μF
Z-Source Inductor	3	mH
DC power supply	180	V

TABLE 2. Parameters of QZSI and PMSM.

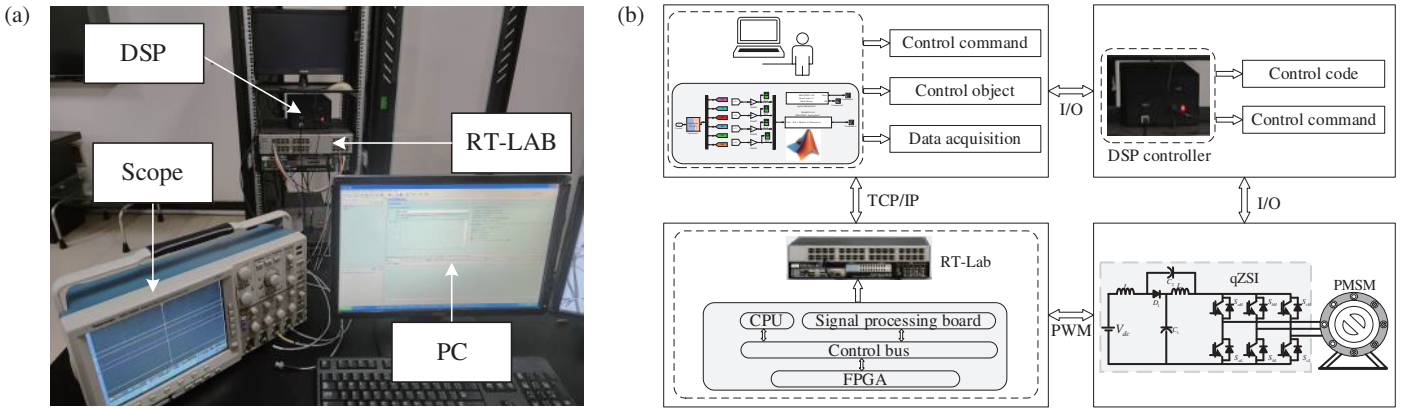

FIGURE 9. Experimental platform. (a) RT-LAB experimental platform. (b) RT-LAB in-the-loop system configuration.

To verify the above analysis, comparative experiments are conducted under the same conditions on the conventional MPC (CMPC) strategy, the joint voltage vector-based MPC (JVVMPC) strategy proposed in [7], the virtual vector modulation-based MPC (VVMMPC) strategy, and the VVMMPC with drive signal optimization (DSO-VVMMPC) strategy. In addition, the proposed strategy maintains a constant switch frequency of 4 times in one control cycle, while the traditional strategy switches between 0 and 6 times in one control cycle. For fair comparison, the control period of the JVVMPC and proposed strategy is set to 120 μs, while the control period of CMPC strategy is set to 40 μs.

4.1. Verification of Drive Signal Optimization Method

The reference value of the capacitor voltage v_{C1} is set to remain constant at 240 V, and the reference value of the corresponding DC bus voltage V_{dc} is 300 V. In the initial state, the reference value of the motor speed n^* is 1500 rpm; the load torque T_L is 12N·m; the load torque is mutated to 16N·m in 0.4 s; and the reference value of the speed is mutated to 1800 rpm in 0.7 s. Experimental waveforms of different strategies are shown in Figs. 10–11.

From Fig. 10(a) and Fig. 11(a), it can be seen that there are significant fluctuations in both the inductor current (i_{L1}) and q-axis stator current (i_q) when the CMPC strategy is applied. Among them, the ripple of i_{L1} is 3.72 A, 4.18 A, 4.19 A; the ripple of i_q is 5.69 A, 6.04 A, 5.93 A; and the total harmonic distortion (THD) of the a-phase current (i_a) is 2.62%, 2.34%, and 2.51%, respectively. After a sudden change in the reference value of the speed, the motor speed follows its reference value after 24.0 ms. From Fig. 10(b) and Fig. 11(b), it can be seen that when using the JVVMPC strategy, the ripple of i_{L1} is 3.48 A, 3.83 A, 4.18 A; the ripple of i_q is 4.65 A, 5.01 A, 5.23 A; and the THD of i_a is 2.29%, 1.88%, and 2.03%, respectively. The motor speed follows its reference value after 24.0 ms when a sudden change occurs. When using the proposed VVMMPC strategy, it can be observed from Fig. 10(c) and Fig. 11(c) that the ripple of i_{L1} and q-axis stator current is significantly reduced. Among them, the ripple of i_{L1} is 3.14 A, 3.02 A, and 3.41 A; the ripple of i_q is 4.06 A, 4.18 A, and 4.50 A; and the THD of i_a is 2.00%, 1.43%, and 1.63%, respectively. After a sudden change in the reference value of the speed, the motor speed follows its reference value after 23.8 ms.

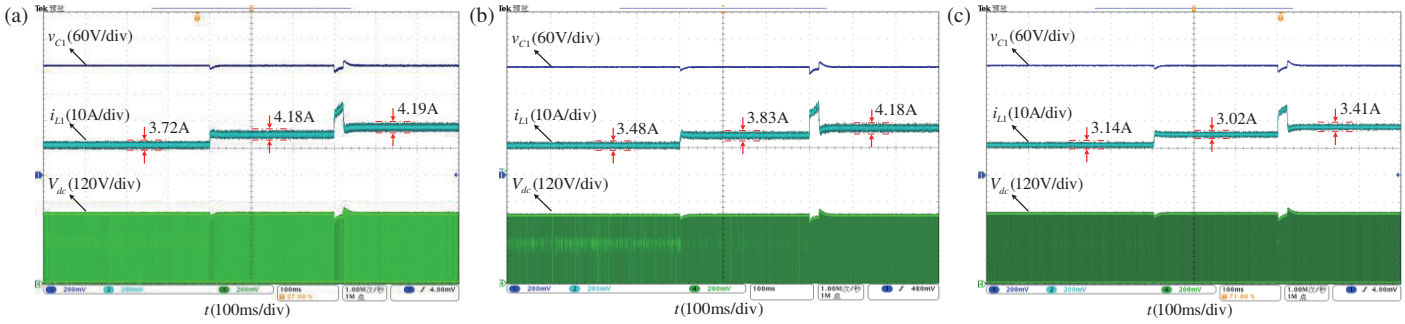

FIGURE 10. Experimental waveforms of QZSI ($V_{dc}^{*} = 300$ V). (a) CMPC strategy. (b) JVVMPC strategy. (c) VVMMPC strategy.

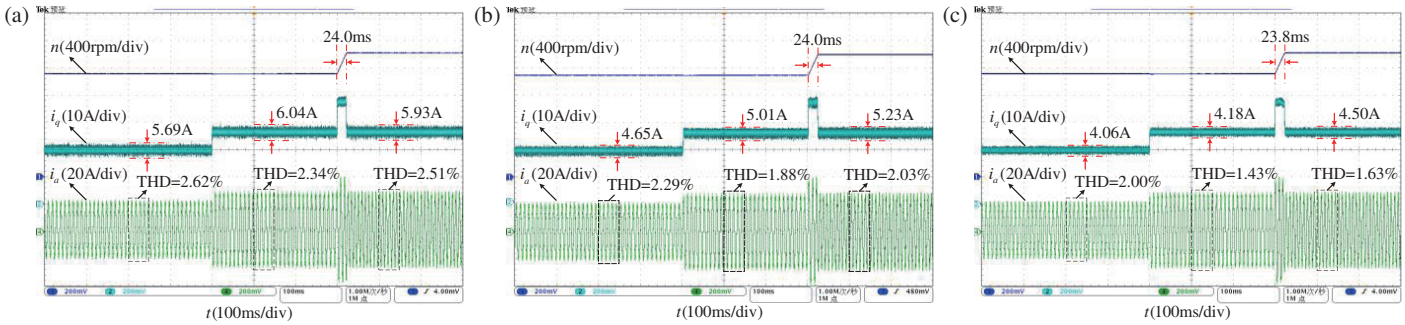

FIGURE 11. Experimental waveforms of PMSM ($V_{dc}^{*} = 300$ V). (a) CMPC strategy. (b) JVVMPC strategy. (c) VVMMPC strategy.

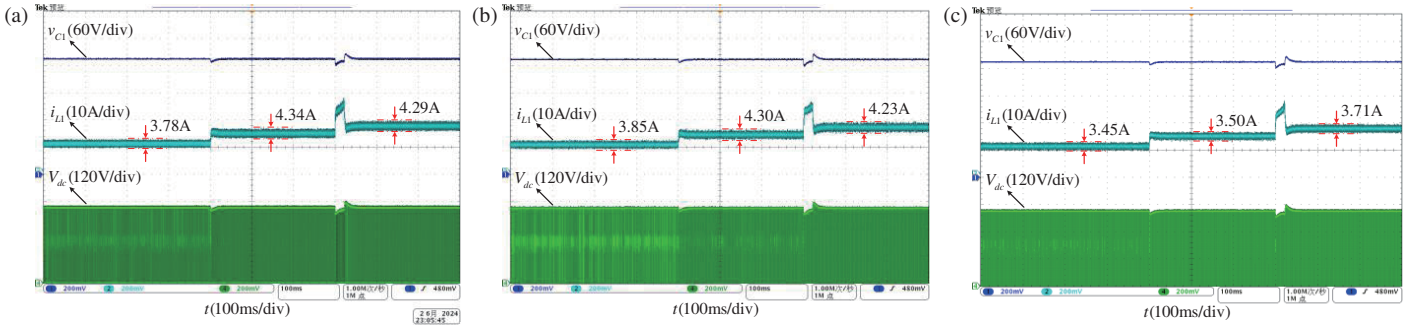

FIGURE 12. Experimental waveforms of QZSI ($V_{dc}^{*} = 330$ V). (a) CMPC strategy. (b) JVVMPC strategy. (c) VVMMPC strategy.

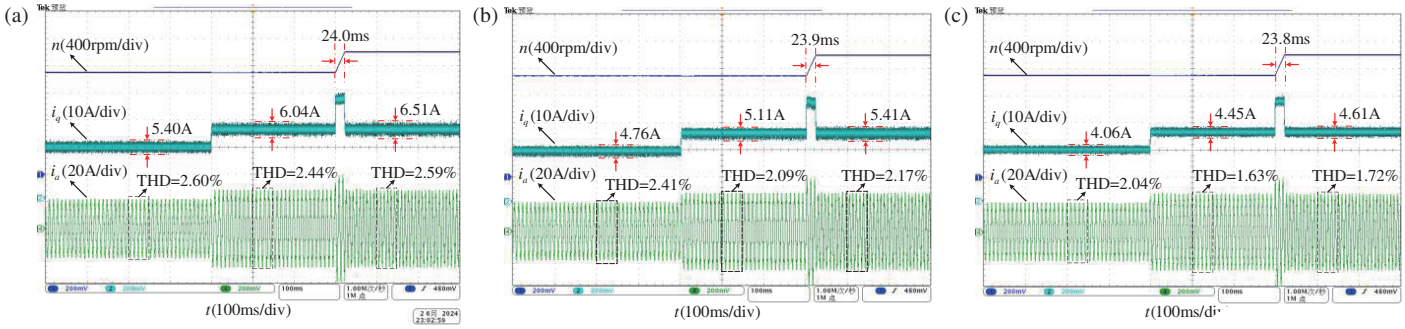

FIGURE 13. Experimental waveforms of PMSM ($V_{dc}^{*} = 330$ V). (a) CMPC strategy. (b) JVVMPC strategy. (c) VVMMPC strategy.

All other conditions remain unchanged. The reference value of v_{C1} is set to remain constant at 255 V, and the corresponding reference value of V_{dc} is 330 V. The comparative experiment between CMPC strategy and VVMMPC strategy is conducted again, and the experimental results are shown in Figs. 12–13.

From Fig. 12(a) and Fig. 13(a), it can be seen that when the CMPC strategy is applied, the ripple of i_{L1} is 3.78 A, 4.34 A, 4.29 A; the ripple of i_q is 5.40 A, 6.04 A, 6.51 A; and the THD of i_a is 2.6%, 2.44%, and 2.59%, respectively. From Fig. 12(b) and Fig. 13(b), it can be seen that when using the JVVMPC

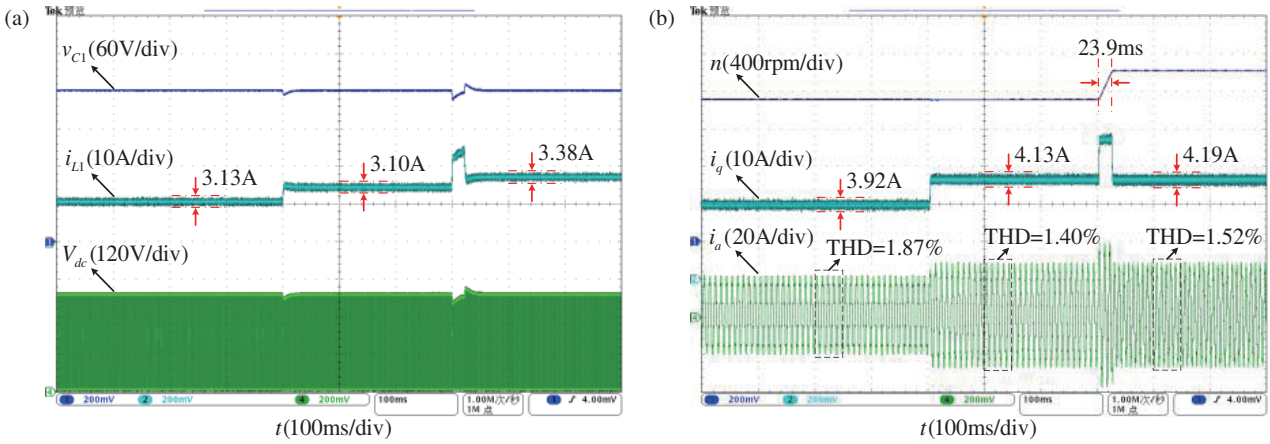

FIGURE 14. Experimental waveforms by DSO-VVMMPC strategy ($V_{dc}^{*} = 300$ V). (a) QZSI. (b) PMSM.

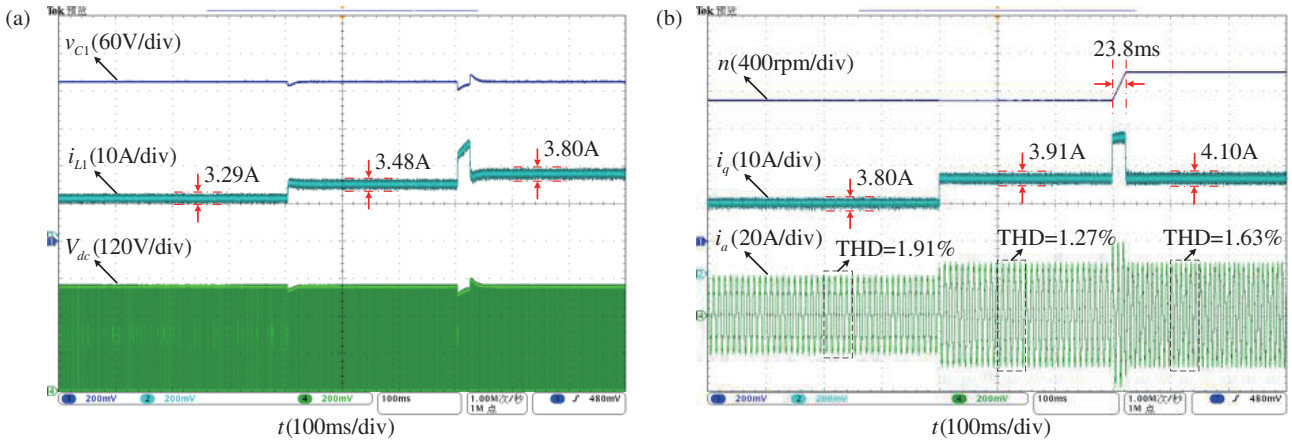

FIGURE 15. Experimental waveforms by DSO-VVMMPC strategy ($V_{dc}^{*} = 330$ V). (a) QZSI. (b) PMSM.

strategy, the ripple of i_{L1} is 3.85 A, 4.30 A, 4.23 A; the ripple of i_q is 4.76 A, 5.11 A, 5.41 A; and the THD of i_a is 2.41%, 2.09%, and 2.17%, respectively. When using the proposed VVMMPC strategy, it can be observed from Fig. 12(c) and Fig. 13(c) that the ripple of i_{L1} is 3.45 A, 3.50 A, and 3.71 A; the ripple of i_q is 4.06 A, 4.18 A, and 4.50 A; and the THD of i_a is 2.04%, 1.63%, and 1.72%, respectively.

Compared with the CMPC and JVVMPC strategies, the VVMMPC strategy using virtual vector modulation can achieve better steady-state performance, with significantly reduced ripples of i_{L1}, i_q and the THD of i_a. It is proven that the strategy of directly calculating the driving signal through the deadbeat algorithm is feasible and effective, greatly reducing the computational burden of the control system without sacrificing computational accuracy.

4.2. Verification of Drive Signal Optimization Method

To verify the accuracy of the proposed drive signal optimization method, the DSO-VVMMPC strategy is experimentally verified under the same conditions, and the experimental results are shown in Figs. 14–15.

When the reference value of v_{C1} is 240 V, and proposed DSO-VVMMPC strategy is used, it can be seen from Figs. 14(a) and (b) that the ripple of i_{L1} is 3.13 A, 3.10 A, and 3.38 A; the ripple of i_q is 3.92 A, 4.13 A, and 4.19 A; the THD of i_a is 1.87%, 1.40%, and 1.52%, respectively. After a sudden change in the reference value of the speed, the motor speed follows its reference value after 23.9 ms. When the reference value of v_{C1} is 255 V, it can be seen from Figs. 15(a) and (b) that the ripple of i_{L1} is 3.29 A, 3.48 A, and 3.80 A; the ripple of i_q is 3.80 A, 3.91 A, and 4.1 A; the THD of i_a is 1.91%, 1.27%, and 1.63%, respectively.

Compared with the proposed VVMMPC strategy, the ripple of i_{L1} in the DSO-VVMMPC strategy that optimizes the driving signal is almost identical. This is because in the design of the experiment, the theoretical calculation value of the through rate d_{sh} is 0.2 and 0.227, respectively, and the driving signal of ST VV is exactly 4 times and 4.5 times of the minimum pulse width. Due to the small changes in the driving signal, the improvement effect of the proposed driving signal optimization method is not significant.

In addition, compared with the proposed VVMMPC strategy, the ripple of i_q and the THD of i_a in proposed DSO-VVMMPC strategy have been improved to varying degrees, which proves

TABLE 3. Comparison of steady-state effects under three control strategies.

Operating conditions		Control variables	CMPC	JVVMPC	VVMMPC	DSO-VVMMPC
$v_{C1}* = 240\,\mathrm{V}$	$T_L = 10\mathrm{N{\cdot}m}$ $n* = 1500\,\mathrm{rpm}$	$\Delta i_{L1}(\mathrm{A})$	3.72	3.48	3.14	3.13
		$\Delta i_q(\mathrm{A})$	5.69	4.65	4.06	3.92
		$i_a\mathrm{THD}(\%)$	2.62	2.29	2.00	1.87
	$T_L = 15\mathrm{N{\cdot}m}$ $n* = 1500\,\mathrm{rpm}$	$\Delta i_{L1}(\mathrm{A})$	4.18	3.83	3.02	3.10
		$\Delta i_q(\mathrm{A})$	6.04	5.01	4.18	4.13
		$i_a\mathrm{THD}(\%)$	2.34	1.88	1.43	1.40
	$T_L = 15\mathrm{N{\cdot}m}$ $n* = 1800\,\mathrm{rpm}$	$\Delta i_{L1}(\mathrm{A})$	4.19	4.18	3.41	3.38
		$\Delta i_q(\mathrm{A})$	5.93	5.23	4.50	4.19
		$i_a\mathrm{THD}(\%)$	2.51	2.03	1.63	1.52
$v_{C1}* = 255\,\mathrm{V}$	$T_L = 10\mathrm{N{\cdot}m}$ $n* = 1500\,\mathrm{rpm}$	$\Delta i_{L1}(\mathrm{A})$	3.78	3.85	3.45	3.29
		$\Delta i_q(\mathrm{A})$	5.40	4.76	4.06	3.80
		$i_a\mathrm{THD}(\%)$	2.60	2.41	2.04	1.91
	$T_L = 15\mathrm{N{\cdot}m}$ $n* = 1500\,\mathrm{rpm}$	$\Delta i_{L1}(\mathrm{A})$	4.34	4.30	3.50	3.48
		$\Delta i_q(\mathrm{A})$	6.40	5.11	4.45	3.91
		$i_a\mathrm{THD}(\%)$	2.44	2.09	1.63	1.27
	$T_L = 15\mathrm{N{\cdot}m}$ $n* = 1800\,\mathrm{rpm}$	$\Delta i_{L1}(\mathrm{A})$	4.29	4.23	3.71	3.80
		$\Delta i_q(\mathrm{A})$	6.51	5.41	4.61	4.10
		$i_a\mathrm{THD}(\%)$	2.59	2.17	1.72	1.63

TABLE 4. Summary of three control methods.

Strategy	CMPC	JVVMPC	VVMMPC	DSO-VVMMPC
Code execution time	0.053 ms	0.050 ms	0.033 ms	0.035 ms
Switching frequency	5.60 kHz	5.40 kHz	5.55 kHz	5.55 kHz
Prediction times	8	3	1	1
Ripple of i_{L1}	high	middle	low	low
Ripple of i_q	high	middle	low	lower
i_a THD	high	middle	low	lower

that this strategy can reduce the total error of driving signal and improve the accuracy of deadbeat algorithm. It is consistent with the theoretical analysis in Subsection 3.3.

The control effects of different control strategies under multiple operating conditions are summarized in Table 3.

The characteristics of different control strategies are summarized in Table 4. It can be seen that the switching frequencies of the three control strategies are almost the same, and the code execution time and prediction frequency of the proposed strategy are shorter.

5. CONCLUSION

Aiming at the issues of drive signal errors and high computational complexity in conventional model predictive control, the DSO-VVMMPC strategy for QZSI-PMSM system is proposed in this paper. It can be concluded that the suggested method has the following advantages verified by theoretical analysis and experiments.

1) Compared with the CMPC strategy, the proposed VVMMPC strategy has better control effect due to the application of virtual vector modulation method. The average reduction in the ripples of i_{L1}, i_q and the THD of i_a is 17.26%, 27.31%, and 30.98%, respectively.

2) Compared with the CMPC strategy, the proposed VVMMPC and DSO-VVMMPC strategies directly calculate the driving signals, which reduces code execution time and the number of control system predictions.

3) The impact of the minimum pulse width on the accuracy of the deadbeat algorithm has been effectively reduced by the proposed drive signal optimization method. Compared with the VVMMPC strategy, the proposed DSO-VVMMPC strategy reduces the ripples of i_q by an average of 4.49% and reduces the THD of i_a by an average of 8.18%.

ACKNOWLEDGEMENT

This work was supported by the Natural Science Foundation of Hunan Province of China under Grant Number 2023JJ50191.

REFERENCES

[1] Boduroglu, A., Y. Demir, B. Cumhur, and M. Aydin, "A novel track structure of double-sided linear PM synchronous motor for low cost and high force density applications," *IEEE Transactions on Magnetics*, Vol. 57, No. 2, 1–5, Feb. 2021.

[2] Zhang, W., Z. Zhang, L. Wen, W. Jiang, X. Gu, and Y. Li, "Multi-gain online autotuning technique-based discrete-time current regulator for permanent magnet synchronous motors," *IEEE Transactions on Power Electronics*, Vol. 39, No. 1, 260–269, Jan. 2024.

[3] Zhang, X., Y. Cao, and C. Zhang, "Model predictive voltage control for PMSM system with low parameter sensitivity," *IEEE Transactions on Industrial Electronics*, Vol. 71, No. 11, 13 601–13 613, Nov. 2024.

[4] Liang, W., X. Mu, Y. Shen, and H. Li, "Inductor current ripple reduction strategy based on two-domain space vector PWM for qusai-Z source inverter," *Transactions of China Electrotechnical Society*, Vol. 40, No. 2, 488–503, 2024.

[5] Agrawal, S., B. Tyagi, V. Kumar, and P. Sharma, "Digital Controller Design and Implementation for AC and DC Side of 3ph qZSI," *IEEE Transactions on Industry Applications*, Vol. 60, No. 1, 672–683, Jan.–Feb. 2024.

[6] Wu, C., J. Yang, and Q. Cheng, "Sequential-model predictive control for quasi-Z-source inverter," *Proceedings of the CSEE*, Vol. 41, No. 12, 4286–4297, 2021.

[7] Xu, Y., Y. He, H. Li, and H. Xiao, "Model predictive control using joint voltage vector for quasi-Z-source inverter with ability of suppressing current ripple," *IEEE Journal of Emerging and Selected Topics in Power Electronics*, Vol. 10, No. 1, 1108–1124, Feb. 2022.

[8] Duan, X., L. Kang, H. Zhou, and Q. Liu, "Multivector model predictive power control with low computational burden for grid-tied quasi-z-source inverter without weighting factors," *IEEE Transactions on Power Electronics*, Vol. 37, No. 10, 11 739–11 748, Oct. 2022.

[9] Battiston, A., E.-H. Miliani, S. Pierfederici, and F. Meibody-Tabar, "Efficiency improvement of a quasi-Z-source inverter-fed permanent-magnet synchronous machine-based electric vehicle," *IEEE Transactions on Transportation Electrification*, Vol. 2, No. 1, 14–23, Mar. 2016.

[10] Dong, S., Q. Zhang, W. Zhang, C. Zhou, and T. Na, "A compound control strategy for improving the dynamic characteristics of the DC-link voltage for the PMSM drive system based on the quasi-Z-source inverter," *IEEE Access*, Vol. 7, 151 929–151 938, 2019.

[11] Xiao, S., X. Gu, Z. Wang, T. Shi, and C. Xia, "A novel variable DC-link voltage control method for PMSM driven by a quasi-Z-source inverter," *IEEE Transactions on Power Electronics*, Vol. 35, No. 4, 3878–3890, Apr. 2020.

[12] Sarker, M. T. and G. Ramasamy, "Optimal signal design in system identification for model predictive control (MPC)," *IEEE Access*, Vol. 11, 140 229–140 237, 2023.

[13] Shadaei, M., J. Khazaei, and F. Moazeni, "Data-driven nonlinear model predictive control for power sharing of inverter-based resources," *IEEE Transactions on Energy Conversion*, Vol. 39, No. 3, 2018–2031, Sep. 2024.

[14] Mahmoudi, H., M. Aleenejad, and R. Ahmadi, "Modulated model predictive control for a Z-source-based permanent magnet synchronous motor drive system," *IEEE Transactions on Industrial Electronics*, Vol. 65, No. 10, 8307–8319, Oct. 2018.

[15] Mahmoudi, H., M. Aleenejad, and R. Ahmadi, "Torque ripple minimization for a permanent magnet synchronous motor using a modified quasi-Z-source inverter," *IEEE Transactions on Power Electronics*, Vol. 34, No. 4, 3819–3830, Apr. 2019.

[16] Pandiya, G. P. and A. Vidyarthi, "A survey on H∞ control-based output feedback techniques," *Engineering, Technology & Applied Science Research*, Vol. 13, No. 5, 11 517–11 523, 2023.

[17] Pandiya, G. P., A. Vidyarthi, and A. Pahadia, "New approach to design optimal robust controller for a 2-D discrete system: OPTIMAL ROBUST CONTROLLER FOR A 2-D DISCRETE SYSTEM," *Journal of Scientific & Industrial Research (JSIR)*, Vol. 84, No. 1, 99–106, 2025.

[18] Yang, L., H. Li, J. Huang, Z. Zhang, and H. Zhao, "Model predictive direct speed control with novel cost function for SMPMSM drives," *IEEE Transactions on Power Electronics*, Vol. 37, No. 8, 9586–9595, Aug. 2022.

[19] Dong, K., T. Shi, S. Xiao, X. Li, and C. Xia, "Finite set model predictive control method for quasi-Z source inverter-permanent magnet synchronous motor drive system," *IET Electric Power Applications*, Vol. 13, No. 3, 302–309, 2019.

[20] Zhou, Z., C. Xia, Y. Yan, Z. Wang, and T. Shi, "Torque ripple minimization of predictive torque control for PMSM with extended control set," *IEEE Transactions on Industrial Electronics*, Vol. 64, No. 9, 6930–6939, Sep. 2017.

[21] Wang, Y., X. Wang, W. Xie, F. Wang, M. Dou, R. M. Kennel, R. D. Lorenz, and D. Gerling, "Deadbeat model-predictive torque control with discrete space-vector modulation for PMSM drives," *IEEE Transactions on Industrial Electronics*, Vol. 64, No. 5, 3537–3547, May 2017.

[22] Agoro, S. and I. Husain, "Robust deadbeat finite-set predictive current control with torque oscillation and noise reduction for PMSM drives," *IEEE Transactions on Industry Applications*, Vol. 58, No. 1, 365–374, Jan.-Feb. 2022.

[23] Wang, Y., S. Huang, W. Liao, J. Zhang, and S. Huang, "IPMSM model predictive current control method based on a novel virtual vector modulation method," *Transactions of China Electrotechnical Society*, Vol. 39, No. 08, 2422–2433, 2024.

[24] Xiao, Q., Z. Yu, W. Zhang, Z. Tang, and Z. Cheng, "Hybrid-vector model predictive flux control for PMSM considering narrow pulse," *Progress In Electromagnetics Research C*, Vol. 137, 235–249, 2023.

[25] Liu, J.-M., Z.-Y. Ge, X. Wu, G.-P. Wu, S.-P. Xiao, and K.-Y. Huang, "Predictive current control of permanent magnet synchronous motor based on duty-cycle modulation," *Proceedings of the CSEE*, Vol. 40, No. 10, 3319–3328, 2020.

[26] Zhang, Y., K. Cao, W. Yi, Y. Meng, and Z. Cheng, "Three-phase duty cycle modulation-based model predictive control strategy for QZSI-PMSM system without cost function," *Progress In Electromagnetics Research C*, Vol. 148, 205–217, 2024.